Minimized open-circuit voltage reduction in GaAs/InGaAs quantum well solar cells with bandgap-engineered graded quantum well depths

Xiaohan Li, Vaishno D. Dasika, Ping-Chun Li, Li Ji, Seth R. Bank, and Edward T. Yu

Citation: Applied Physics Letters **105**, 123906 (2014); doi: 10.1063/1.4896739
View online: http://dx.doi.org/10.1063/1.4896739
View Table of Contents: http://scitation.aip.org/content/aip/journal/apl/105/12?ver=pdfcov
Published by the AIP Publishing

Minimized open-circuit voltage reduction in GaAs/InGaAs quantum well solar cells with bandgap-engineered graded quantum well depths

Xiaohan Li, Vaishno D. Dasika, Ping-Chun Li, Li Ji, Seth R. Bank, and Edward T. Yu
Microelectronics Research Center, University of Texas at Austin, 10100 Burnet Rd., Austin, Texas 78758, USA

(Received 16 July 2014; accepted 16 September 2014; published online 26 September 2014)

The use of InGaAs quantum wells with composition graded across the intrinsic region to increase open-circuit voltage in *p-i-n* GaAs/InGaAs quantum well solar cells is demonstrated and analyzed. By engineering the band-edge energy profile to reduce photo-generated carrier concentration in the quantum wells at high forward bias, simultaneous increases in both open-circuit voltage and short-circuit current density are achieved, compared to those for a structure with the same average In concentration, but constant rather than graded quantum well composition across the intrinsic region. This approach is combined with light trapping to further increase short-circuit current density. © *2014 AIP Publishing LLC*. [http://dx.doi.org/10.1063/1.4896739]

The trade-off between the open-circuit voltage (V_{oc}) and short-circuit current density (J_{sc}) of a solar cell requires the optimum bandgap of a conventional *pn* junction solar cell to fall approximately between 1.3 eV and 1.6 eV.[1–3] The bandgap of GaAs is squarely in this range and power conversion efficiency as high as 28.8% has been achieved for a single-junction GaAs solar cell.[4] The efficiency of *pn* junction solar cells can potentially be further improved by insertion of low-dimensional nanostructures, e.g., quantum wells (QWs), into a GaAs *p-i-n* photovoltaic cell structure so that J_{sc} can be increased by extending the cell's absorption to longer wavelengths (>900 nm).[5–9] However, reports show that such approaches often result in a reduced V_{oc}, as material defects can be introduced due to lattice mismatch[10,11] and carrier extraction efficiency can be lowered since QWs can function as recombination centers for photo-generated carriers.[12–14] To mitigate these effects, strain-balance techniques have been employed to minimize lattice relaxation during growth.[15,16] Other approaches have involved designing different band-edge energy profiles, such as stepped potential barriers in QW solar cells, to increase photo-generated carrier extraction efficiency.[17]

In this letter, we demonstrate and analyze a bandgap-engineered design for thin-film *p-i-n* GaAs/InGaAs QW solar cells with indium concentration monotonically changing from 10% to 30% through the intrinsic region to maintain a high V_{oc}. By engineering the band-edge energy profile, the photo-generated carrier concentration in the QWs is reduced at large forward bias, and both V_{oc} and J_{sc} are increased compared to a QW cell with the same average indium concentration but constant QW composition across the intrinsic region. For QW cells in this study, long-wavelength optical absorption in the QW region is further improved by increasing the light path inside the thin-film semiconductor layer using light trapping techniques,[18–20] in which backscattering structures were fabricated via a nanosphere lithography (NSL) process.[21]

Sample structures were grown by solid-source molecular beam epitaxy (MBE) on GaAs (001) undoped substrates and are shown schematically in Figure 1. For each sample, a 200 nm n-type GaAs buffer layer was grown, followed by an 800 nm n-type ($n \sim 2 \times 10^{18}\,cm^{-3}$) $Al_{0.85}Ga_{0.15}As$ etch stop layer, 20 nm n-type ($n \sim 6.5 \times 10^{18}\,cm^{-3}$) GaAs contact layer, and 30 nm n-type ($n \sim 3 \times 10^{18}\,cm^{-3}$) $Al_{0.85}Ga_{0.15}As$ window layer. A 100 nm n-type ($n \sim 3 \times 10^{18}\,cm^{-3}$) GaAs emitter layer was grown next, followed by an unintentionally doped layer consisting of either 134 nm GaAs (structure (i)) or GaAs/InGaAs QW structures (structures (ii)–(v)) with a total intrinsic region thickness of 134 nm. A 2000 nm p-type (Be-doped, $p \sim 5 \times 10^{18}\,cm^{-3}$) GaAs base layer, a 100 nm p-type ($p \sim 1 \times 10^{18}\,cm^{-3}$) $Al_{0.2}Ga_{0.8}As$ back surface field layer and a 20 nm thick p-type ($p \sim 5 \times 10^{18}\,cm^{-3}$) GaAs contact layer then completed each epitaxial layer structure. The growth temperature was kept above 500 °C throughout. For intrinsic GaAs, the background doping concentration from impurities in the chamber is below the threshold of Hall measurements, and is therefore estimated to be below $10^{-15}\,cm^{-3}$. Band-edge energy diagrams of QW cells at forward bias were computed using a 1D Poisson solver,[22] with constant separation of electron and hole Quasi-Fermi levels (QFL) throughout the intrinsic region assumed. Current-voltage characteristics were measured using normally incident light from a Newport Oriel 96 000 solar simulator operating at 1-sun illumination with an airmass (AM) 1.5G filter. Photocurrent response spectra were measured at zero bias using a single grating monochromator based system from Optronic Laboratories with AC lock in detection.

Key device fabrication processes are illustrated in Figures 2(a)–2(d). A 100 nm SiO_2 layer was e-beam evaporated onto the epitaxially grown p^+-GaAs surface, followed by patterning using the NSL process, in which 500 nm diameter polystyrene spheres were deposited on the SiO_2 surface in a hexagonal array using a Langmuir-Blodgett process[23] (Figure 2(a)). Reactive-ion etching was used to shrink the sphere diameter to 250 nm, followed by deposition of 15 nm Cr, a lift-off process in which the polystyrene spheres were dissolved in toluene under sonication, and then reactive-ion etching of the SiO_2 with a CF_4/O_2 gas mixture (Figure 2(b)). 10 nm Cr/40 nm Au/1200 nm In metallization was then deposited to form the nanostructured rear contact (Figure 2(c)). Then, using a home-built wafer-bonding apparatus, the cell structure was flip-bonded to a silicon substrate on which

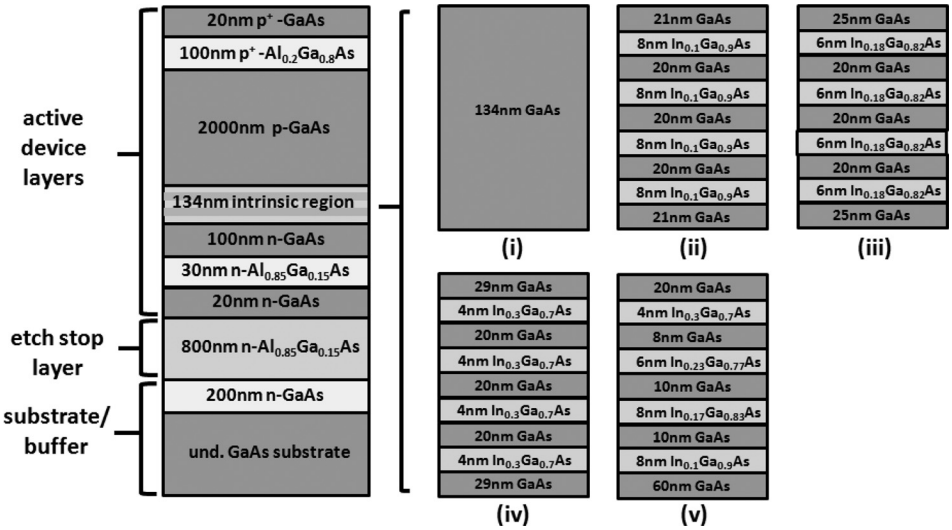

FIG. 1. Schematic diagrams of epitaxial layer structures for (i) GaAs *pn* homojunction cell structure; (ii) GaAs/$In_{0.1}Ga_{0.9}As$ QW cell structure; (iii) GaAs/$In_{0.18}Ga_{0.82}As$ QW cell structure; (iv) GaAs/$In_{0.3}Ga_{0.7}As$ QW cell structure; and (v) graded QW cell structure. Active device layers, etch stop layers, and substrate/buffer layers labeled for each correspond to similarly labeled sample layers in Figure 2.

10 nm Cr/800 nm Au had previously been deposited by e-beam evaporation. Finally, substrate removal and mesa etching processes were employed to create 1 mm × 1 mm and 2 mm × 2 mm device mesas on the silicon supporting substrates, and the devices were coated with a 76 nm silicon nitride antireflection coating (Figure 2(d)). Additional details regarding the thin-film device fabrication process used in this work have been reported elsewhere.[20,24]

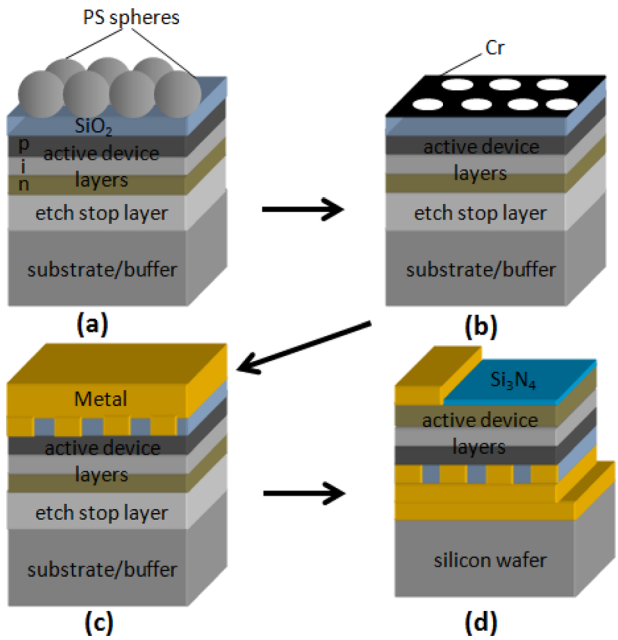

FIG. 2. Key steps in process flow for fabrication of complete thin-film solar cell devices integrated with nanostructured metal/dielectric rear contacts bonded onto silicon substrates. (a) 100 nm SiO_2 layer was deposited on the cell surface using e-beam evaporation, followed by a NSL process, in which a hexagonal array of 500 nm diameter polystyrene sphere was created on the SiO_2 surface. (b) A Cr hard mask was created after polystyrene sphere diameter shrinking using reactive-ion etching, followed by e-beam deposition of 15 nm Cr, and a lift-off process in which polystyrene spheres were dissolved in toluene under sonication. (c) The nanostructured rear contact was formed by e-beam deposition of 10 nm Cr/40 nm Au/1200 nm In metallization. (d) The cell structure was flip-bonded to a silicon substrate on which 10 nm Cr/800 nm Au metallization had previously been e-beam deposited, and 1 mm × 1 mm and 2 mm × 2 mm device mesas were created after a substrate removal and mesa etching process, and coated with a 76 nm silicon nitride antireflection coating.

The key idea for the graded QW cell structure design is that it enables increased separation of the electron QFL from the QW conduction band-edge at forward bias, resulting in a reduced photo-generated carrier concentration in the QWs at forward bias and, consequently, increased V_{oc} and operating voltage for maximum power output. At the same time, for the graded QW cell structure, the QW barriers can be substantially thinner, compared to those in reference QW cells with the same maximum In content, while remaining below the critical thickness for strain relaxation so that tunneling transport of carriers is facilitated. For GaAs/InGaAs QWs, the conduction band offsets are significantly larger than the valence band offsets, making electrons more difficult to be collected than holes.[25] As a result, in this study, the design focused on the QW solar cell conduction band-edge energy diagrams to demonstrate the basic concept.

Figure 3(a) shows a 1D Poisson calculation of the band-edge energy diagram for the GaAs/$In_{0.1}Ga_{0.9}As$ QW cells under a forward bias of 0.8 V. It is anticipated that if there exists significant overlap of the electron QFL with the QW conduction band states, carrier collection efficiency will be greatly reduced due to the high concentration of photo-generated carriers trapped inside the QWs, and a V_{oc} as high as 0.8 V cannot be maintained. For the GaAs/$In_{0.1}Ga_{0.9}As$ quantum well reference cell, which has the shallowest set of QWs, a small overlap of the electron QFL with the InGaAs conduction band states can be observed, but it is a relatively minor factor in determining the cell's V_{oc} due to the lower electronic density of states in the conduction band of GaAs/$In_{0.1}Ga_{0.9}As$ QWs compared to QWs with higher In concentration. Figures 3(b) and 3(c) show band-edge energy diagrams computed using the 1D Poisson solver for GaAs/$In_{0.18}Ga_{0.82}As$ and GaAs/$In_{0.3}Ga_{0.7}As$ QW cells at 0.8 V forward bias, respectively. The electron QFL is well above the conduction band-edge energy for at least one QW in each case, which suggests that at a forward bias of 0.8 V, a significant concentration of photo-generated carriers is trapped inside the QWs instead of being extracted, resulting in a degraded V_{oc}. Figure 3(d) shows the simulated band-edge energy diagram of the graded QW cell at 0.8 V forward bias. The electron QFL is very clearly below the conduction band-edge energy for all the QWs in this structure, which ensures

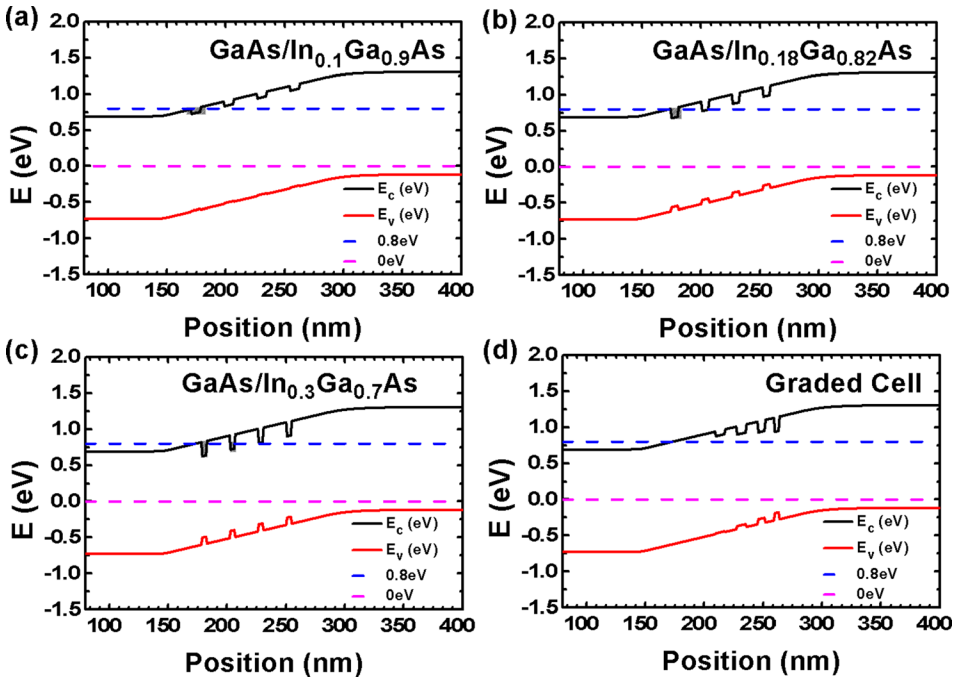

FIG. 3. 1D Poisson simulation results of bandgap-edge energy diagrams for (a) $GaAs/In_{0.1}Ga_{0.9}As$ QW cell; (b) $GaAs/In_{0.18}Ga_{0.82}As$ QW cell; (c) QW cell with graded QW depths; and (d) $GaAs/In_{0.3}Ga_{0.7}As$ QW cell under the forward bias of 0.8 V. Grey areas indicate regions that electron QFL stays above the QW conduction band-edge.

that a low photo-generated carrier concentration is trapped in the QWs at 0.8 V forward bias. We note that with regard to carrier concentrations in the QWs, the assumption that the electron QFL is constant across the intrinsic region is essentially the most conservative assumption, and the actual carrier concentrations in the QWs can be lower.[26–28] However, the graded QW design enables the electron QFL to stay well below the QW conduction band-edge, resulting in a reduced QW carrier concentration, at large forward bias voltages. Here, the average indium concentration for the graded QW solar cell is taken to be 18%, and is calculated via averaging the QW compositions weighted by the thickness of each QW

$$18\% = \frac{10\% \times 8\,\text{nm} + 17\% \times 8\,\text{nm} + 23\% \times 6\,\text{nm} + 30\% \times 4\,\text{nm}}{8\,\text{nm} + 8\,\text{nm} + 6\,\text{nm} + 4\,\text{nm}} \quad (1)$$

which is a more conservative estimate compared to simply averaging over the indium concentration for each QW, which would yield an average concentration of 20%.

Figure 4(a) shows current-voltage characteristics under AM1.5G, 1-sun illumination for the GaAs homojunction and GaAs/InGaAs QW cells integrated with nanostructured rear contacts. Figure 4(b) shows external quantum efficiency (E.Q.E.) measurements for the full set of devices, including the homojunction and QW cells integrated with nanostructured rear contacts. The $GaAs/In_{0.3}Ga_{0.7}As$ QW cell yields the highest E.Q.E. at wavelengths longer than 900 nm, for which optical absorption occurs only in the QW region. However, the largest degradation in V_{oc} is also observed for the $GaAs/In_{0.3}Ga_{0.7}As$ QW cell. The graded QW cell shows slightly lower E.Q.E. at wavelengths longer than 900 nm compared to the $GaAs/In_{0.3}Ga_{0.7}As$ QW cell, but significantly higher E.Q.E. compared to the other QW cells and the homojunction cell, and maintains E.Q.E. larger than 4% up to 980 nm, significantly exceeding the 1% E.Q.E. per QW level typically observed.[29] We note that because of the strong excitonic absorption near the QW absorption edge,[30] combined with strong coupling of incident light to a guided mode in the thin-film semiconductor structure at ~930 nm, the measured and simulated E.Q.E. in this wavelength range, as well as the measured value for J_{sc}, for the GaAs/$In_{0.1}Ga_{0.9}As$ QW cell is unusually high compared to those for the other QW samples. These observations are consistent

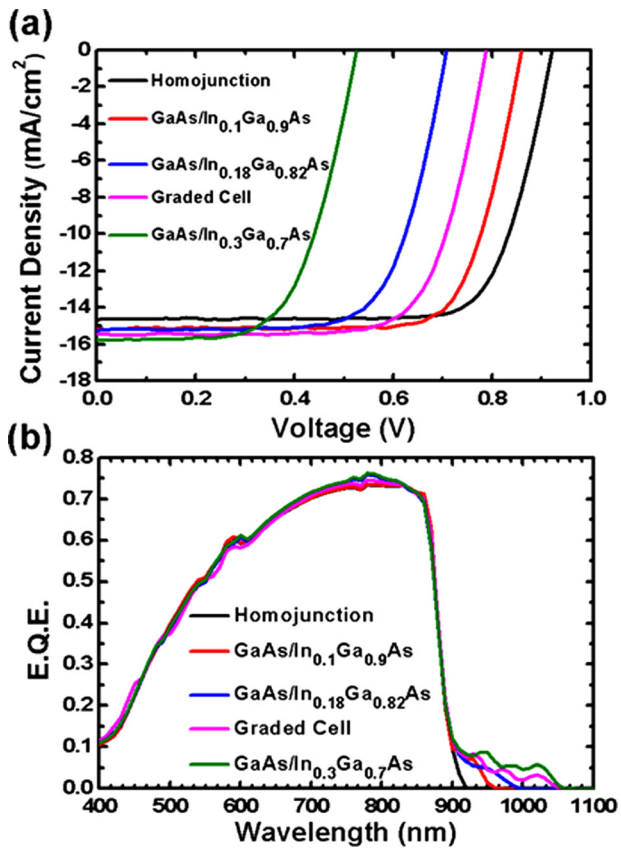

FIG. 4. (a) Current density-voltage characteristics measured under AM1.5G 1-sun illumination from a solar simulator for a GaAs *p-i-n* homojunction cell, and for GaAs/InGaAs QW cells with nanostructured rear contacts. (b) Measured E.Q.E. for the full set of devices.

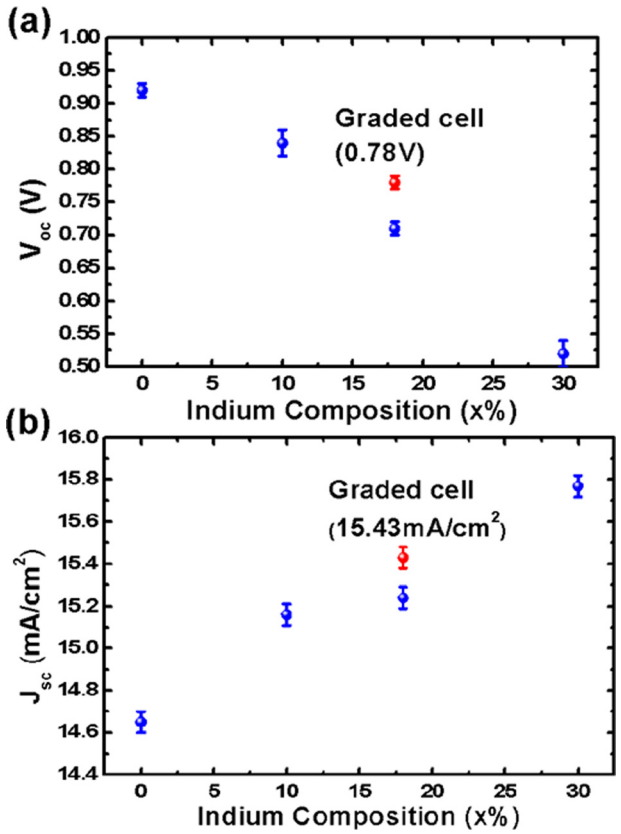

FIG. 5. (a) and (b) Measured V_{oc} and J_{sc} versus QW indium content of each cell, respectively.

with predictions derived from the 1D Poisson simulation results described above.

Figures 5(a) and 5(b) show the measured V_{oc} and J_{sc}, respectively, of the full set of devices versus the QW indium concentration in this study. For the graded QW cell, the QW In concentration is taken to be the average In concentration in the four QWs present in the device. For the homojunction, GaAs/$In_{0.1}Ga_{0.9}As$, GaAs/$In_{0.18}Ga_{0.82}As$, and GaAs/$In_{0.3}Ga_{0.7}As$ QW reference cells, a steady decrease in V_{oc} from 0.92 V to 0.52 V is observed with increasing indium content in the QWs. This trend is consistent with other works that have been reported.[31,32] Similarly, the fill factor decreases slightly with increasing In concentration in the QW solar cells.[33,34] For the measurements shown in Figure 4(a), the fill factors are 76.9% for the GaAs homojunction reference cell, 76.1% for the GaAs/$In_{0.1}Ga_{0.9}As$ QW solar cell, 71.3% for the GaAs/$In_{0.18}Ga_{0.82}As$ cell, and 63.7% for the GaAs/$In_{0.3}Ga_{0.7}As$ cell. The graded cell has a slightly higher fill factor, 73.8%, than the GaAs/$In_{0.18}Ga_{0.82}As$ cell, which has the same average In concentration in the quantum wells. In addition, the graded QW cell, with an average 18% indium concentration in the QWs, shows both improved V_{oc} (70 mV increase) and J_{sc} (0.21 mA/cm^2 increase) compared to the GaAs/$In_{0.18}Ga_{0.82}As$ QW cell. Taking this behavior for the GaAs/$In_{0.1}Ga_{0.9}As$ QW cell into account, we see that use of the graded QW device structure enables both V_{oc} and J_{sc} to be increased, simultaneously, beyond the trend lines observed for GaAs/InGaAs QW cells with constant In concentration in the QWs.

In summary, we have demonstrated a bandgap-engineering strategy for GaAs/InGaAs thin-film QW solar cells with graded QW depths, which is shown to increase both V_{oc} and J_{sc} compared to a QW solar cell with uniform QW composition at the same average composition as the graded-well structure. 1D Poisson simulations of band-edge energy diagrams show that for the graded QW cell, the electron QFL separation from the QW conduction band-edge under a forward bias near its V_{oc} is increased compared to QW cells with uniform composition across the intrinsic region, which effectively reduces photo-generated carrier concentration in the QWs. Measurements show that V_{oc} of the homojunction and QW cells with constant QW composition decreases significantly with increasing indium content in the QWs, while the graded QW cell, with an average 18% indium concentration in the QWs, shows improvement in both V_{oc} and J_{sc} compared to the GaAs/$In_{0.18}Ga_{0.82}As$ QW cell. The integration of light trapping structures with the QW solar cells provides increased optical absorption at the longer wavelengths (>900 nm) for which absorption occurs only in the QWs, and for the graded QW cell, it is measured to extend longer wavelength absorption up to 1050 nm while maintaining a greater than 1% E.Q.E. per QW up to 980 nm. This approach thus shows promise for further improving the performance of QW cells, particularly for those with deep QWs, in terms of maintaining both high V_{oc} and J_{sc} values under solar illumination. We anticipate that V_{oc} of the graded structure may be further improved by thinning the QW barriers or employing other strategies to further increase photo-generated carrier tunneling transport, thereby increasing the carrier extraction efficiency. This approach may also be implemented in more complex QW systems, such as ternary or quaternary QWs, where large conduction and valence band offsets can simultaneously be achieved by adjusting the QW material composition to further increase the range of absorbed wavelengths while maintaining a minimal reduction in V_{oc}.

Part of this work was supported by the National Science Foundation (ECCS-1120823 and DMR-1311866), the Air Force Office of Scientific Research (FA9550-10-1-0182), and the Judson S. Swearingen Regents Chair in Engineering at the University of Texas at Austin.

[1]R. C. Knechtli, R. Y. Loo, and G. S. Kamath, IEEE Trans. Electron Devices **31**, 577 (1984).
[2]W. Shockley and H. Queisser, J. Appl. Phys. **32**, 510 (1961).
[3]C. H. Henry, J. Appl. Phys. **51**, 4494 (1980).
[4]M. A. Green, K. Emery, Y. Hishikawa, W. Warta, and D. Dunlop, Prog. Photovoltaics **22**, 1–9 (2014).
[5]K. Barnham, I. Ballard, J. Barnes, J. Connolly, P. Griffin, B. Kluftinger, J. Nelson, E. Tsui, and A. Zachariou, Appl. Surf. Sci. **113/114**, 722 (1997).
[6]D. Derkacs, W. V. Chen, P. M. Matheu, S. H. Lim, P. K. L. Yu, and E. T. Yu, Appl. Phys. Lett. **93**, 091107 (2008).
[7]D. B. Bushnell, N. J. Ekins-Daukes, K. W. J. Barnham, J. P. Connolly, J. S. Roberts, G. Hill, R. Airey, and M. Mazzer, Sol. Energy Mater. Sol. Cells **75**, 299 (2003).
[8]K. Tanabe, K. Watanabe, and Y. Arakawa, Appl. Phys. Lett. **100**, 192102 (2012).
[9]M. F. Bennett, Z. S. Bittner, D. V. Forbes, S. R. Tatavarti, S. P. Ahrenkiel, A. Wibowo, N. Pan, K. Chern, and S. M. Hubbard, Appl. Phys. Lett. **103**, 213902 (2013).
[10]R. Dahal, J. Li, K. Aryal, J. Y. Lin, and H. X. Jiang, Appl. Phys. Lett. **97**, 073115 (2010).
[11]J. C. Zolper and A. M. Barnett, IEEE Trans. Electron Devices **37**, 478–484 (1990).

[12]K. W. J. Barnham, B. Braun, J. Nelson, M. Paxman, C. Button, J. S. Roberts, and C. T. Foxon, Appl. Phys. Lett. **59**, 135 (1991).
[13]N. G. Anderson, J. Appl. Phys. **78**, 1850 (1995).
[14]R. Corkish and M. A. Green, in *Proceedings of 23rd IEEE Photovoltaic Specialists Conference* (1993), p. 675.
[15]P.-H. Wu, Y.-K. Su, I.-L. Chen, C.-H. Chiou, J.-T. Hsu, and W.-R. Chen, Jpn. J. Appl. Phys., Part 1 **45**, 25 (2006).
[16]Y. Wang, S. Ma, K. Watanabe, M. Sugiyama, and Y. Nakano, J. Cryst. Growth **352**, 194–198 (2012).
[17]Y. Wen, Y. Wang, K. Watanabe, M. Sugiyama, and Y. Nakano, IEEE J. Photovoltaics **2**, 221–226 (2012).
[18]V. E. Ferry, J. N. Munday, and H. Atwater, Adv. Mater. **22**, 4794 (2010).
[19]X. H. Li, P. C. Li, D. Z. Hu, D. Schaadt, and E. T. Yu, J. Appl. Phys. **114**, 044310 (2013).
[20]P. Spinelli, V. E. Ferry, J. van de Groep, M. van Lare, M. A. Verschuuren, R. E. I. Schropp, H. A. Atwater, and A. Polman, J. Opt. **14**, 024002 (2012).
[21]C. L. Haynes and R. P. Van Duyne, J. Phys. Chem. B **105**, 5599 (2001).
[22]G. Snider, 1D Poisson Program (PC version beta 8), University of Notre Dame, see http://www.nd.edu/~demand.
[23]J. Rybczynski, U. Ebels, and M. Giersig, Colloids Surf. **219**, 1 (2003).
[24]X. H. Li, P. C. Li, D. Z. Hu, D. Schaadt, and E. T. Yu, J. Appl. Phys. **115**, 044303 (2014).
[25]Y. Yanezawa, T. Kitatani, J. Minemura, K. Tamura, and T. Warabisako, in *Proceedings of 24th IEEE Photovoltaic Specialists Conference* (1994), p. 1878.
[26]M. Courel, J. Rimada, and L. Hernandez, Prog. Photovoltaics **21**, 276 (2013).
[27]U. Rau, Phys. Rev. B **76**, 085303 (2007).
[28]N. J. Ekins-Daukes, C. D. J. Calder, I. Ballard, K. W. J. Barnham, J. Nelson, J. S. Roberts, and G. Hill, in *Proceedings of 3rd World Conference on Photovoltaic Energy Conversion* (2003), p. 2702.
[29]D. B. Bushnell, T. N. D. Tibbits, K. W. J. Barnham, J. P. Connolly, M. Mazzer, N. J. Ekins-Daukes, J. S. Roberts, G. Hill, and R. Airey, J. Appl. Phys. **97**, 124908 (2005).
[30]C. O. McPheeters, D. Hu, D. M. Schaadt, and E. T. Yu, J. Opt. **14**, 024007 (2012).
[31]X. Zhang, X. Wang, H. Xiao, C. Yang, Q. Hou, H. Yin, H. Chen, and Z. Wang, Chin. Phys. B **20**, 028402 (2011).
[32]I. Serdiukova, C. Monier, M. F. Vilela, and A. Freundlich, Appl. Phys. Lett. **74**, 2812 (1999).
[33]K. Y. Lai, G. J. Lin, Y.-L. Lai, Y. F. Chen, and J. H. He, Appl. Phys. Lett. **96**, 081103 (2010).
[34]R. Dahal, B. Pantha, J. Li, J. Y. Lin, and H. X. Jiang, Appl. Phys. Lett. **94**, 063505 (2009).